Development of a 4π detection system for the measurement of the shape of β spectra

Abhilasha Singh, Xavier Mougeot, Sylvain Leblond, Martin Loidl, Benoit Sabot, Abdel Nourreddine

Development of a 4π detection system for the measurement of the shape of β spectra

A. Singh[a], X. Mougeot[a], S. Leblond[a], M. Loidl[a], B. Sabot[a] and A. Nourreddine[b]

[a] Université Paris-Saclay, CEA, List, Laboratoire National Henri Becquerel (LNE-LNHB), F-91120 Palaiseau, France
[b] Institut Pluridisciplinaire Hubert Curien, Université de Strasbourg, CNRS-IN2P3-UMR 7178, 23 rue du Loess, BP 28, F-67037, Strasbourg Cedex 2, France

ARTICLE INFO

Keywords:
^{14}C beta spectrum
^{204}Tl beta spectrum
Si detectors
4π detection
Experimental shape factor
Monte Carlo simulation

ABSTRACT

The need of precise measurements of the energy distribution of emitted β particles has been addressed developing a specific detection system. An ultra-thin radioactive source, prepared on purpose, is enclosed between two silicon detectors in a compact geometry with a quasi-4π sr solid angle. The remaining distortions have been corrected with a dedicated deconvolution process based on mono-energetic Monte Carlo simulations that are used to build the response matrix. The β spectra from ^{14}C and ^{204}Tl decays have been measured and analysed. Extracted maximum energies are fully consistent with the AME2020 recommended Q-values. A linear slope of a = -0.430 (23) MeV^{-1} that comes from the weak magnetism term in ^{14}C spectrum has been determined, in excellent agreement with the theoretical predictions. Knowledge of the ^{204}Tl spectrum has been extended down to 60 keV and a shape factor ($dq^2 + \lambda_2 p^2$) has been extracted with d = 1.075 (7).

1. Introduction

Beta (β) decays have always played a major role in fundamental physics. Being at the origin of the discovery of the neutrino (ν), the study of this three-body disintegration remains very relevant today. The energy distribution of β particles is still scrutinized in the search of new physics beyond the Standard Model [1, 2] or to investigate the antineutrino reactor anomaly [3]. A precise knowledge of β spectra is also pivotal for other scientific communities like radionuclide metrology for standardizing activity measurements [4, 5], nuclear energy industry for decay heat calculations [6], or nuclear medicine for internal vectorized radiotherapy [7].

Despite such a wide panel of applications, experimental knowledge on the shape of β spectra is quite limited. The vast majority of the studies were performed before the 1970's with apparatuses that were struggling to achieve good accuracy. Most of the measurement limitations were due to the escape of particles, to back-scattering, and to self-absorption in the radioactive sources [8, 9]. In addition, these studies were primarily focused on allowed and first forbidden β transitions, covering only a limited range among all the β transitions [10].

Nuclear data wise, β decay properties have been calculated with the LogFT code [11] for the last 50 years in the evaluations, either from ENSDF [12] or DDEP [13]. The BetaShape code has been developed over the past decade with improved models in order to provide more detailed and accurate information [14]. Any allowed or forbidden unique transition can be treated while forbidden non-unique transitions, which are very sensitive to nuclear structure, are approximated as allowed or unique transitions of the same variation of total angular momentum [10]. Each transition type exhibits its own shape factor $C(W)$ that enters the definition of the β spectrum:

$$\frac{dN}{dW} \propto pWq^2F(Z,W)C(W)R(Z,W)r(Z,W)dW \quad (1)$$

where p and q are the β and ν particle momenta, respectively. From the kinetic energy E of the β particle and m_e its rest mass, one usually defines its total energy $W = 1 + E/m_e$ and $p = \sqrt{W^2 - 1}$. The maximum transition energy E_0 is defined from the Q-value and the energies of the initial and final nuclear states. Correspondingly, one thus defines W_0 from E_0 and $q = W_0 - W$. The Fermi function $F(Z,W)$ accounts for the static Coulomb field generated by the nucleus, while $R(Z,W)$ stands for the radiative corrections and $r(Z,W)$ for the atomic overlap correction. Recently, a specific version of this code has been developed to include realistic nuclear structure information for the study of the first forbidden non-unique transitions in ^{151}Sm decay [15]. However as shown in [10], many more high-precision measurements of β spectra would be necessary to constrain and validate the theoretical predictions.

To address this need, a dedicated detection system has been developed recently at the Laboratoire National Henri Becquerel (LNE-LNHB) to provide precise measurements of the shape of β spectra. The setup has been optimized using Monte Carlo simulations to reach a quasi-4π geometry by sandwiching a radioactive source between two silicon detectors [16]. Special care has been taken to develop a procedure reducing as much as possible the self-absorption in the sources.

The apparatus, the procedure for radioactive source preparation and the Monte Carlo simulations are described in section 2. The characterisation of the device has been performed by measuring ^{109}Cd and ^{207}Bi sources and is presented in section 3. To benchmark the detection system capability, the β spectra from the ^{14}C allowed decay and from the ^{204}Tl first

*abhilasha.singha@ganil.fr
**xavier.mougeot@cea.fr
ORCID(s):

forbidden unique decay have been measured. The spectra have been corrected from distortions due to various phenomena: escape of particles, self-absorption in the source, dead-layer, etc. A specific unfolding algorithm has been developed based on a complete Monte-Carlo simulation of the detection system, detailed in section 4. Finally, the analysis of the corrected spectra is presented in section 5: extraction of the maximum energies and of the shape factors; comparison with published measurements and theoretical predictions.

2. Detection system

We have developed an apparatus dedicated to the precise measurement of electron spectrum shapes, primarily for β^- decays. Electron (back-)scattering is the physical phenomenon that contributes most to the distortion of the measured spectrum. To minimize its influence, we have optimized the setup to obtain a close to 4π geometrical acceptance in order to absorb as much as possible the emitted energy from the decay.

The detection system has been built upon two Si detectors that were chosen for their good energy resolution and easy handling. Passivated Implanted Planar Silicon (PIPS®) detectors from MIRION Technologies [17] have been selected among those commercially available. Electron spectroscopy benefits from their ultra-low dead layer in the entrance window, with a thickness equivalent to 50 nm Si, minimizing any loss of kinetic energy before detection. The active volume, fully depleted, is a cylindrical Si crystal with 1 mm thickness and 300 mm^2 surface area. It is encapsulated by the manufacturer in an aluminum housing with a 0.9 mm gap between the metal surface and the silicon surface. The detectors have been arranged in holders facing each other, the radioactive source clamped in between and each preamplifier placed next to the radial connector for output signal (see Figure 1 and 2). This configuration allows a collection of the β particles in an almost 4π solid angle.

2.1. Optimization of geometry

The detector holder was designed with the SOLIDWORKS software[18]. The main difficulty was to find the optimal configuration to avoid any radioactive contamination of the Si detectors while keeping them as close to each other as possible to minimize the escape of scattered β particles. The whole detection assembly is a four-piece copper holder consisting of two parts for placing the detectors and two closing plates. A specific notch in the center of both detector holders enables a repeatable positioning of the radioactive source, visible on Figure 2b.

Taking into account all the technical constraints, a distance of 2.5 mm between the two detectors was achieved (Figure 1), which corresponds to a geometrical factor of 98.7%. Monte Carlo simulations have been performed for this compact geometry varying this distance and quantifying the influence on the β spectra [19].

Furthermore, the entire assembly is placed in an ultra-vacuum chamber and cooled at 100 K with liquid nitrogen. A copper finger is dedicated to cooling, on which the detection assembly is fixed thanks to the cylindrical structure visible on Figure 2c. A hole in the center of the holder, visible on the front edge on Figure 2a,b, serves as a chimney to ensure fast vacuuming around the radioactive source.

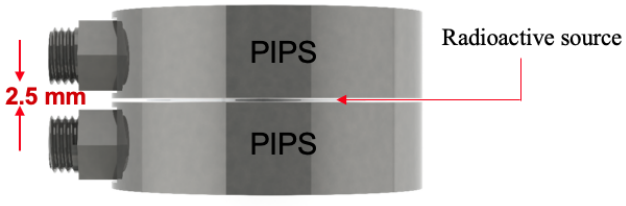

Figure 1: Scheme of two planar detectors with a radioactive source in middle.

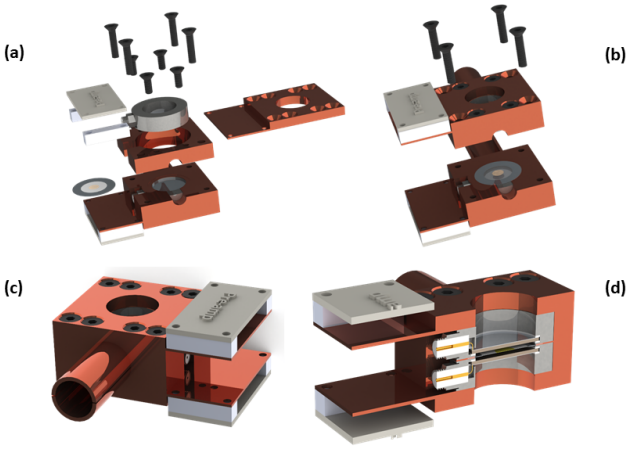

Figure 2: 3D picture of the detection system. (a) An exploded view of the pieces of the detection system. (b) Two detectors in their respective detector holder. (c) The whole detection system in measurement configuration. (d) A cut view in the middle of the detection system.

2.2. Signal acquisition

Each detector is associated with a low-noise, fast rise-time charge-sensitive A1422H preamplifier from CAEN [20]. We selected a model designed to be used up to 200 pF capacitance, well suited for out detectors of 31.5 pF, with a sensitivity of 90 $mV{\cdot}MeV^{-1}$. The preamplifier is placed at a 3 cm distance from the detector, which significantly reduces the cable capacitance and hence increases the signal-to-noise ratio.

Data have been acquired with a nanoMCA labZY module [21], which includes a real-time digital pulse processor and a high-performance digital multichannel analyzer. This module supports a variety of radiation detectors and takes as input the signal from the preamplifier. Signal processing can easily be optimized through various shaping parameters. However, this module does not provide any list-mode possibility that would allow for parallel acquisition of the signals

from the two detectors. We thus decided to directly sum the signals right after the preamplifiers. Even if the detectors and preamplifiers are in principle identical, the signal analysis on the oscilloscope showed a slight difference of gain for an identical reference energy peak. To adjust this gain mismatch between the two signals, an in-house passive module was implemented that also sums up the signal without adding any significant noise component. The gain adjustment was performed very accurately by measuring the conversion electron peaks at 481 keV and 975 keV from ^{207}Bi decay. The summed signal is then sent to the nanoMCA module for acquisition.

2.3. Radioactive source preparation

Due to their small rest mass, β particles scatter very easily in the matter. The quality of the radioactive source is thus of utmost importance in any precise measurement of a β spectrum. It has been known for decades that the spectrum shape can be significantly distorted because of source thickness or chemical crystallization [22, 23]. The self-absorption of electrons in the source support has been already discussed in a previous study [19]. The film used as support has to be as thin as possible, the radioactive deposit has to be homogeneously distributed and the crystallization has to be controlled to minimize crystals size.

A specific preparation technique has been developed to produce ultra-thin radioactive sources perfectly suitable for β spectrometry. The source support is a 0.7 µm thick Mylar® film glued on a stainless steel ring of 150 µm thickness. Latex microspheres of 70 nm mean diameter are electrosprayed in the center of the film on a 10 mm diameter area, visible in Figure 3. A drop of radioactive solution, prepared beforehand with optimal concentration, is precisely weighed and next deposited with a micropipette. The microspheres serve as a seeding agent for the crystallization process and increase the wettability of the film, what maintains the deposit at the center and ensures its homogeneity during the drying process. After many tests, the best source quality was found to be obtained using a freeze-drying process [24], which allows fast and homogeneous crystallization. The source is eventually shielded with a second 0.7 µm thick Mylar® film to prevent contamination. Typical activity of the source was chosen around 1 kBq to limit dead time and possible pile-up events. The source placement within the detection system is shown in Figure 4.

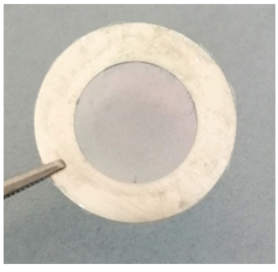

Figure 3: A Mylar® film source support with electrosprayed latex microspheres.

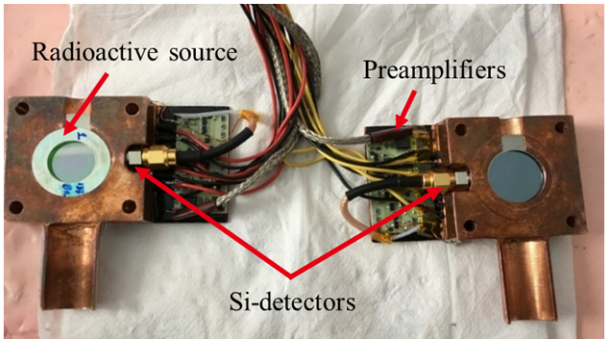

Figure 4: Experimental set-up with two PIPS® detectors (300 mm^2) in a configuration close to 4π geometry and preamplifiers fixed with Stycast® Epoxy glue.

2.4. Monte Carlo simulations

Simulations of the current setup have been performed with the PENELOPE 2014 Monte Carlo code [25], which is well known for its accurate model of photon, electron and positron transport in matter, especially at low energy. A detailed geometry was implemented including a complete description of the detectors with their dead layers, of the source material and thickness, and of the copper holder.

Some parameters can influence the computational burden of the simulation, but also its accuracy. The absorption energy E_{abs} fixes the minimum energy absorbed in the material. The constant C_1 allows for an adjustment of the mean free path between two hard collisions, while the average fractional loss of energy between two hard collisions can be adjusted with the constant C_2. Finally, the energies W_{cc} and W_{cr} correspond to the cutoff energies of hard elastic collisions and hard bremsstrahlung emission, respectively. In the top panel of the Figure 5, a comparison of two simulated β spectra is shown for the same geometry and the same ^{14}C theoretical spectrum as input, but with different set of parameters. The lowest energy values give in principle the most accurate result, which is in excellent agreement with the spectrum generated from the second set of parameters.

To quantify this agreement, one can look at the distribution of the standardized residuals. Let's consider a set of n measurements $\{y_i\}$, a model resulting in n predictions $\{y_i^{th}\}$ and the model error defined by their difference $\hat{e}_i = y_i - y_i^{th}$. The unbiased variance estimates are given by

$$\mathrm{var}(y_i) = \sum_{i=1}^{n} \frac{(y_i - \overline{y})^2}{n-1} \quad \text{and} \quad \mathrm{var}(\hat{e}_i) = \sum_{i=1}^{n} \frac{(\hat{e}_i)^2}{n-p-1} \tag{2}$$

with $\overline{y}$ the average of the measurements and p the number of model parameters. In our analysis of β spectra, two parameters constrain the model: the normalisation of the simulated data to the experimental data and the maximum energy. The standardized residuals are then defined by

$$r_i = \frac{\hat{e}_i}{\sqrt{\mathrm{var}(\hat{e}_i)}}. \tag{3}$$

If the predicted values from simulation, calculation or fit are relevant, 99.7% of the standardised residuals must fall within

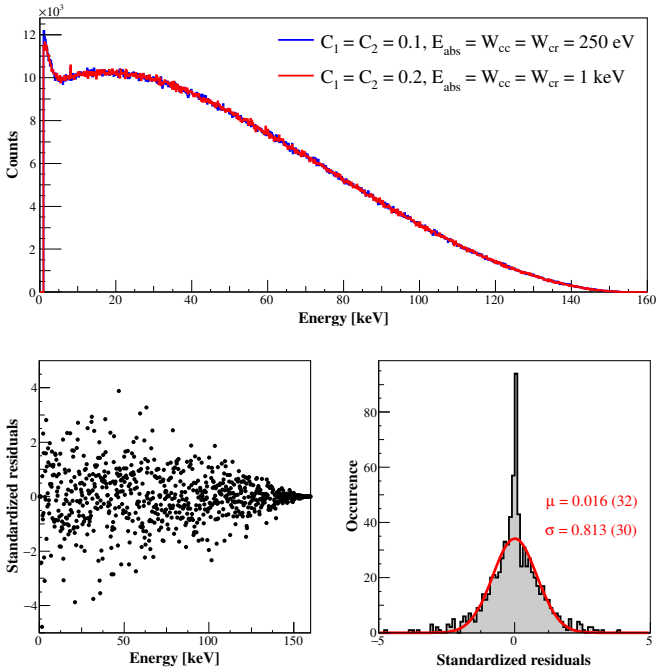

Figure 5: Top panel is the comparison of different input parameters using the almost 4π geometry, with the example of ^{14}C decay. Residuals between the two spectra given is plotted as function of energy on the bottom left panel, and its projection is represented on the bottom right panel.

±3, 95.4% within ±2 and 68.3% within ±1. For later use in this work, we also define the disagreement parameter

$$(1 - R^2) = \frac{\mathrm{var}(\hat{e}_i)}{\mathrm{var}(y_i)}, \tag{4}$$

where R^2 is the coefficient of determination. The quantity $(1 - R^2)$ thus estimates the global disagreement between a measured spectrum and a modeled spectrum.

The residuals between the two spectra are given in the bottom panels of Figure 5. One can clearly see that they are uniformly distributed. We thus kept the second set of parameters with 1 keV energy cutoff for all our simulations, increasing their computational speed and ensuring their accuracy at the same time.

3. Characterization

The detection system has been investigated by analysing the energy peaks from specific sources. The β spectra from ^{14}C and ^{204}Tl decays have been measured and compared to their respective simulations.

Systematic background measurements have been carried out to verify the absence of any radioactive contamination of the detection system due to potential material leakage from the sources. The background spectrum is mostly peaked below 20 keV and its influence on the spectra measured with radioactive sources can be considered as very little. In the energy range of study, the background spectrum accounts only for 0.095% of ^{14}C data, and for 0.080% of ^{204}Tl data respectively. All the measured spectra presented in this work are background subtracted.

3.1. Energy response

The energy response of our detection system was studied by measuring ^{109}Cd and ^{207}Bi radioactive sources prepared on purpose. Their electron peaks cover a large range in energy, from a few keV up to 1 MeV. The decay of ^{109}Cd is characterized by a single γ transition at 88 keV that is highly converted [26]. Atomic Auger electrons are emitted at 22.5 keV, as well as conversion electrons at 62.5 keV from the *K*-shell and at 86.7 keV from the *L*-shell. In ^{207}Bi decay, the electron peaks of interest come from the conversion process in the two main γ transitions at 570 keV and 1064 keV [27]. The former gives electron peaks at 481.6 keV and 553.6 keV, and the latter at 975.6 keV and 1061.7 keV, from the *K*- and *L*-shells respectively. The peaks were fitted using the COLEGRAM software [28]. The energy calibration curve was found very linear, as can be seen in Figure 6. The energy resolution was established to be 9 keV (FWHM) at 62.5 keV, and an energy threshold of 20 keV was determined.

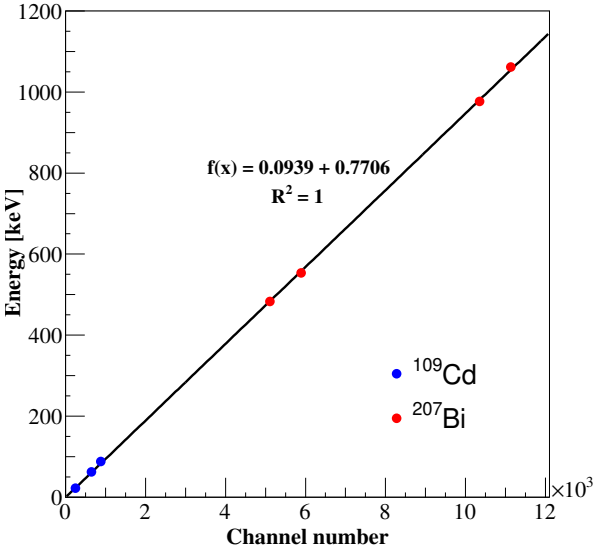

Figure 6: The energy calibration curve obtained from the conversion electron peaks in ^{109}Cd and ^{207}Bi decays.

The calibrated spectrum of ^{207}Bi was compared to a simulation in order to validate the implemented geometry. This simulation was performed using the PenNuc module [25] of PENELOPE, which automatically manages the cascade of particles from the decay scheme (γ-rays, conversion electrons) and the consecutive atomic relaxation (X-rays, Auger electrons) based on DDEP data. The simulated spectrum was enlarged with a Gaussian distribution of 9 keV FWHM, as experimentally determined. The spectra are compared in Figure 7 and have been normalised by integration in the 600-700 keV energy range. Good agreement is obtained,

with a disagreement parameter $(1 - R^2)$ of 3.2%. This non-negligible discrepancy is caused by a small disagreement in the peak intensities. As the simulation is based on decay data in which electron intensities are not measured but calculated, a slight difference with our measurement was considered to be reasonable.

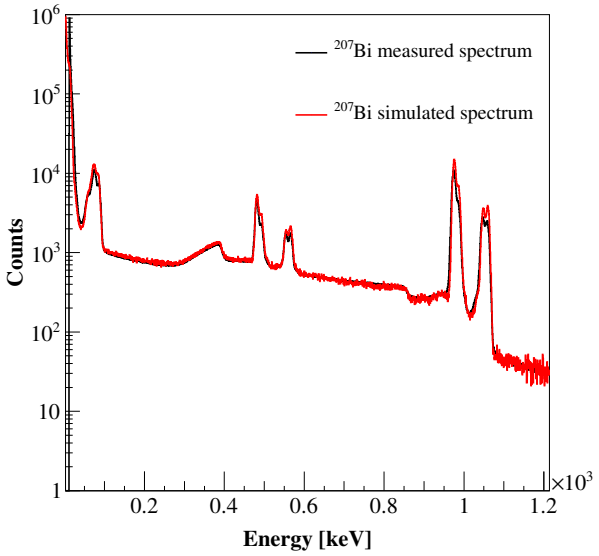

Figure 7: Comparison between the simulated spectrum and the measured spectrum of ^{207}Bi decay.

3.2. Measurements

The first β spectrum that has been measured is from ^{14}C decay, which exhibits a single allowed transition with a maximum energy of $E_0 = 156.476\ (4)$ keV [29] and a half-life of $T_{1/2} = 5\,700\ (30)$ a [30]. It is compared to the result of a simulation in Figure 8, for which a theoretical spectrum from BetaShape was used as input as in section 2. The simulated spectrum has been normalized to the measurement by integration between 25 and 145 keV. Both spectra are in excellent agreement with a disagreement parameter $(1 - R^2)$ of only 0.016% in this energy range.

The second β spectrum is from ^{204}Tl, which decays at 97.08 (13)% through a single first forbidden unique transition, and at 2.92 (13)% via an electron capture of the same nature [31]. The β transition energy is 763.75 (18) keV [29]. Again, a theoretical spectrum from BetaShape was used as input for a simulation. The simulated spectrum has been normalized to the measured spectrum in the 100-750 keV region and their comparison is given in Figure 9. Good agreement is obtained, with a disagreement parameter $(1 - R^2)$ of 0.33%. However, a discrepancy between simulation and measurement can be noticed below 100 keV. The contribution of the electron capture branch is a possible explanation, as it leads to the emission of Auger electrons and X-rays between 53 and 83 keV. Our energy resolution is not sufficient to clearly distinguish the different peaks of low intensity, which could result in extra counts like a bump in the measured spectrum.

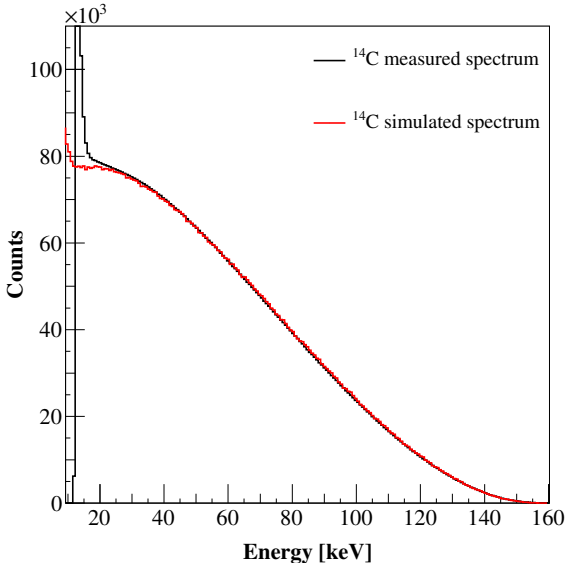

Figure 8: Comparison between the measured (black) and simulated (red) spectra of ^{14}C decay.

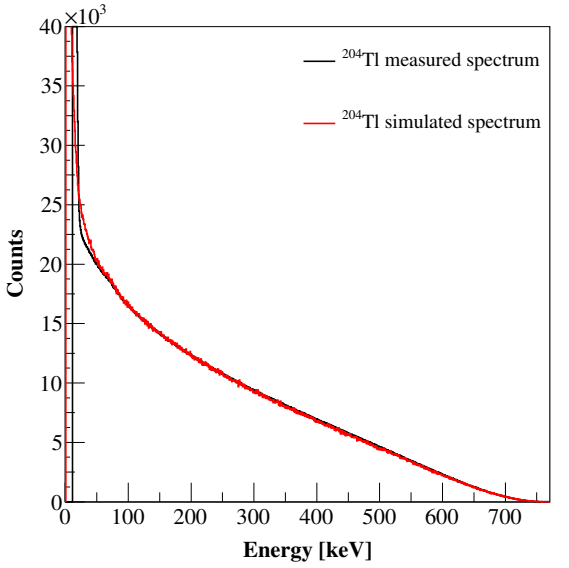

Figure 9: Comparison of the measured spectrum (black) of ^{204}Tl with the simulated spectrum (red). The input of the simulation is the theoretical spectrum calculated from BetaShape.

These two measured spectra still suffer from distortion due to the detection system. Before analysing them further, it is necessary to correct this effect in order to retrieve the kinetic energy spectrum of the β particle as emitted at the nucleus.

4. Deconvolution process

The measured spectrum results from the convolution of the initially emitted spectrum with the response of the detection system, which includes the effect of the source itself.

In order to recover the spectrum free of distortion, it is necessary to determine the response function and to unfold the measured spectrum. The approach used in this study is based on the matrix inversion method, which has been used in several previous studies (see e.g. [32, 33]). The unfolding process is presented below and has been adapted from the work of Paulsen et al. [33], who provided detailed mathematical justifications.

4.1. Method

The solution is exactly as long as the problem is not mathematically ill-posed. The objective is to determine how the content of a given energy bin $[E_i, E_{i+1}[$ is spread over the other bins, and what has been done with mono-energetic simulations. The response matrix of the detection system has thus been built independently of the knowledge of the β spectrum. The unfolded, initially emitted spectrum has then been obtained by applying the inverse of this matrix to the measured spectrum.

An identical binning of $\Delta E = 1$ keV has been considered for all our spectra, which means intervals $[E_i, E_{i+1}[$ with $(E_{i+1}\text{-}E_i) = \Delta E$ starting from $E_0 = 0$ keV. The first bins in the measured spectrum are empty due to the threshold applied to cut the electronic noise. Maximum energy has also been fixed beyond which it is reasonable to consider that no physical information is present, typically a few keV beyond the maximum energy of the β spectrum.

These considerations determine the dimensions of the vectors for the measured and emitted spectra, and of the matrix for the response function. The latter is a square matrix and the measured spectrum $M(E_i)$ results from the multiplication of the response matrix $R(E_i+\Delta E, E_i)$ of the detection system by the initially emitted spectrum $S(E_i)$:

$$\begin{pmatrix} M(E_0) \\ \vdots \\ \vdots \\ \vdots \\ M(E_N) \end{pmatrix} = \begin{pmatrix} R(E_0+\Delta E, E_0) & \cdots & R(E_N+\Delta E, E_0) \\ \vdots & & \vdots \\ \vdots & \ddots & \vdots \\ \vdots & & \vdots \\ R(E_0+\Delta E, E_N) & \cdots & R(E_N+\Delta E, E_N) \end{pmatrix} \times \begin{pmatrix} S(E_0) \\ \vdots \\ \vdots \\ \vdots \\ S(E_N) \end{pmatrix} \tag{5}$$

Each column of the response matrix quantifies how the content of an energy bin is distributed over the other bins. The initial particles emitted with a kinetic energy in the interval $[E_i, E_{i+1}[$ fall in the corresponding bin $S(E_i)$. They partly contribute to the measured number of counts in all the bins with a weight given by the response matrix elements. The latter have been obtained from Monte Carlo simulations considering a series of mono-energetic primary events, one per energy bin. As electrons always loss a small amount of energy in the detector dead layers, what prevents full-energy deposition, only the bins with an energy lower than the primary energy have a non-null content (see Figure 10). All the matrix elements below the diagonal are null and all the diagonal elements are strictly positive. The response matrix is therefore triangular and invertible by construction. In addition, each column of the matrix has been normalised to unity, what keeps information about the absolute number of counts.

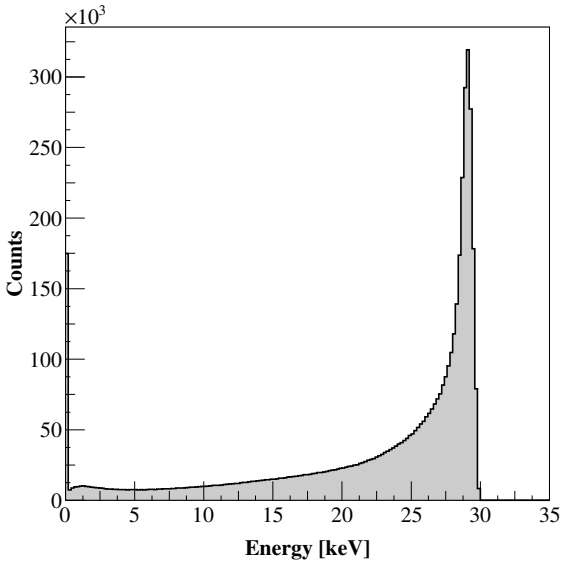

Figure 10: Normalised histogram resulting from a Monte Carlo simulation with primary electrons of 30 keV kinetic energy.

4.2. Validation

Before applying the algorithm to the measured spectrum, it was validated using simulations. Different "measured" spectra – i.e. $M(E_i)$ vectors – were generated by simulation and the unfolding process was then applied to retrieve the original input spectra – i.e. $S(E_i)$ vectors. To minimize the possible statistical effects of the method, the response matrix was generated from mono-energetic pulse simulations with five million primary events for each energy bin. In all the cases performed, the initial spectrum was retrieved with good accuracy down to 10 keV. As the energy threshold of our detection system is above 10 keV, it was concluded that the unfolding process can be confidently applied to our measurements.

It has to be highlighted that this method requires the use of a reliable Monte Carlo model to achieve a trustworthy deconvolution. The accuracy and reliability of our simulations has already been discussed in detail in section 3. In addition, it worth mentioning that the quasi-4π geometry dramatically reduces the magnitude of the unfolding correction and therefore, its contribution to the final uncertainty.

5. Analysis

The deconvolution process described above has been applied to the measured spectra from ^{14}C and ^{204}Tl decays.

5.1. ^{14}C decay

The ^{14}C decay is an allowed transition that exhibits an unusual long half-life. It is a clear sign of an accidental cancellation of the nuclear matrix elements that are generally dominant in such a transition [34]. The question then arises about how much its β spectrum shape is influenced.

On the theory side, different studies concluded that this cancellation increases relatively the influence of the weak

magnetism term. This term appears in the β decay formalism when the nucleons are assumed to have a spatial extension [35]. It adds a dependency in the shape factor linear in the kinetic energy of the β particle:

$$C(E) = 1 + aE \tag{6}$$

The most precise studies available in the literature gave consistent values of a, presented in Table 1. The most recent one from [36] solved a long-standing discrepancy in the $A = 14$ system.

It is noteworthy that these studies considered a numerical Fermi function $F(Z, W)$ determined for a nucleus modeled as a uniform charged sphere, or equivalently an analytical Fermi function for a point nucleus with corrections to account for its finite size. In the present work, we have considered three types of Fermi functions: *i*) F_0 (analytical) for a point nucleus; *ii*) F_0L_0 (numerical) for a uniform charged sphere; and *iii*) $F_0L_0^*$ (numerical) which also includes a screened potential from [37] that takes into account the screening effect due to the atomic electrons.

The β spectrum was investigated with different measurement techniques over the past 70 years (see e.g. [38, 39, 40, 41, 42, 8]). The two most precise studies ([41, 8]) extracted a maximum energy slightly lower than the recommended value, totally dominated by a single high-precision measurement from [43]. However, their extracted shapes are not consistent, as can be seen in Table 1. In [41], a detailed analysis of a measurement carried out with a ^{14}C-doped germanium detector led to a slope consistent with theory. The shape factor used in [8] is different:

$$C(E) = 1 + \beta(E_0 - E) \tag{7}$$

but a and β can easily be deduced from one another:

$$\beta = -a/(1 + aE_0) \tag{8}$$

The measurement was performed with a wall-less gas proportional counter and led to a slope significantly far from the theoretical predictions.

The measured spectrum of ^{14}C presented in Figure 8 has been unfolded from the remaining distortions of the detection system with the method described in the previous section. It is compared in Figure 11 to a high-precision measurement performed by Metallic Magnetic Calorimetry (MMC) several years ago at LNHB [46]. The original 200 eV energy binning of the MMC spectrum has been degraded to match our 1 keV binning. The peaks at low energy are from ^{55}Fe and ^{109}Cd external sources used for energy calibration. The MMC spectrum has been normalized to our measured spectrum by integration in [25,150] keV. Excellent agreement has been found in this energy range with a disagreement parameter $(1 - R^2)$ equal to 0.043%. The corresponding residuals are well distributed around zero within 2σ.

When analyzing a measured β spectrum, the maximum energy and the spectrum shape are somehow correlated because of the q^2 dependency (see Eq. 1). We followed a standard procedure in the literature to extract a shape factor from our measurement. First, we have determined the maximum energy from the Kurie plot. Next, the shape factor has been fitted fixing the maximum energy. The uncertainties we are reporting may be underestimated because they do not include the influence of the energy calibration, the source thickness and the distance between the detectors.

Table 1
Linear slope in ^{14}C shape factor from precise theoretical and experimental studies, compared with the results from the present work. SM stands for shell-model and CVC for the conserved vector current hypothesis.

Study	a in MeV^{-1}	Comment
[44]	-0.386	CVC from exp. not certain
[45]	-0.37 (4)	SM, ×2 difference with CVC
[36]	-0.43	SM, consistent with CVC
[41]	-0.45 (4)	^{14}C-doped Ge detector
[8]	-1.038 (28)	Wall-less prop. counter
This work	-0.430 (23)	Si detector, with F_0L_0
This work	-0.526 (30)	Si detector, with $F_0L_0^*$

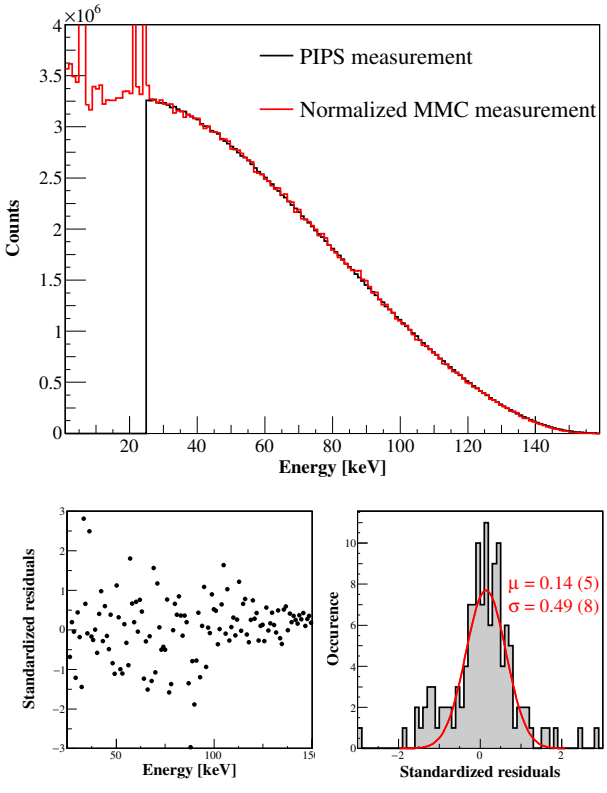

Figure 11: Unfolded ^{14}C spectrum from this work (black) compared to the MMC spectrum measured in [46], normalized between 25 and 150 keV (blue). Residuals are also given in the energy range of the normalization.

The Kurie plot is defined so that it contains mostly a linear dependency in neutrino momentum q close to the maximum energy. The shape factor term $C(W)$ is thus supposed to equal unity. From Eq. 1, one has:

$$\sqrt{\frac{N_{\mathrm{exp}}}{pWF(Z,W)}} = Kq \times \sqrt{r(Z,W)} \tag{9}$$

where K is a constant and N_{exp} is the number of counts in the bin with energy W. The atomic overlap correction has to be kept in the fit as it depends on the maximum energy [47]:

$$r(Z,W) = 1 - B''/q \tag{10}$$

The quantity $B'' = \partial^2 B(G)/\partial Z^2$ is the second derivative of the total electron binding energy of the atom in its ground state and is energy independent. Its value can be estimated from the fit given in [47]. For ^{14}C, one gets $B'' = 92.14$ eV.

The maximum energy is given when the electron takes all the available energy from the decay, i.e. $q = W - W_0 = 0$. The denominator has been convoluted with a Gaussian distribution of 9 keV FWHM to account for the energy resolution of our detection system. A reasonable energy range of [30,150] keV has been considered to determine the central value in order to minimize the influence of a possible non-linearity at the edge of the measured spectrum. To estimate an uncertainty due to the energy range, the lower limit has been varied from 25 to 90 keV and the upper limit from 145 to 155 keV. The uncertainty component due to the fit has been included and we have also considered the variation due to the different Fermi functions. The maximum energy from our measurement is then $E_0 = 156.49\ (43)$ keV. This value has been obtained with the most precise Fermi function that includes screening. Neglecting the overlap correction in the fit would have decreased E_0 by about 40 eV.

As our maximum energy is very consistent with the recommended AME2020 Q-value, the extraction of the shape factor has been done by fixing E_0 to the latter. The theoretical spectrum has been calculated as in Eq. 1 without $C(W)$, next convoluted with a Gaussian distribution to account for the energy resolution, and then normalized to the measured spectrum. The shape factor has been determined by fitting the bin-per-bin ratio of measured to theoretical spectra. A slight non-linear trend has been found, most probably due to our assumption of a constant Gaussian distribution. The maximum energy range to constrain at best the quadratic polynomial fit is [25,145] keV. The lower limit has been varied up to 50 keV and the upper limit from 135 to 150 keV to quantify the influence of the boundaries of the chosen interval. Eventually, a linear coefficient a = -0.430 (23) MeV^{-1} has been determined. The experimental spectrum is shown in Figure 12 together with an allowed theoretical spectrum and the adjusted spectrum. Excellent agreement has been found from 25 to 156 keV with a disagreement parameter $(1 - R^2)$ equal to 0.0014%. The corresponding residuals are well centered around zero within 2σ.

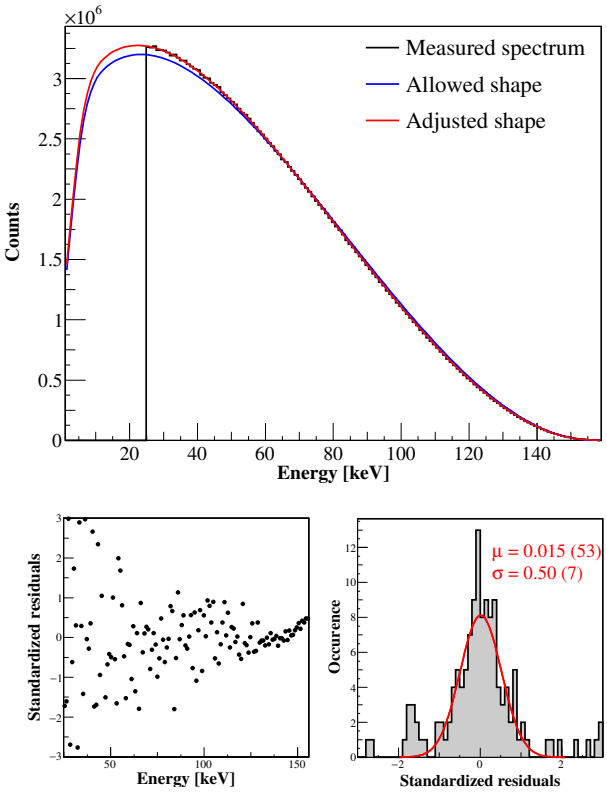

Figure 12: Adjusted ^{14}C spectrum (dashed red) on the unfolded quasi-4π Silicon spectrum from this work (black). The shape has been fitted between 25 and 145 keV starting from an allowed shape (doted blue). Residuals are also given in the energy range from 25 to 156 keV.

Employing the analytical Fermi function F_0 instead of F_0L_0 does not change the extracted shape. However, considering the screened Fermi function $F_0L_0^*$ removes about half of the non-linearity in the ratio spectrum. The linear coefficient is then significantly increased, as shown in Table 1.

5.2. ^{204}Tl decay

The reference ^{204}Tl experimental β spectrum is from Flothmann et al. [48] and was measured more than 50 years ago with a 4π Si(Li) β spectrometer from 190 to 675 keV. Our measurement presented in Figure 9 has an energy threshold much lower but the previously observed discrepancy with the simulation slightly complicates the analysis below 100 keV. As mentioned before, it most probably comes from X-rays and Auger electrons. However, the deconvolution process only accounts for electrons and the detection system is not able to discriminate between photons and electrons. Looking closely at the measured spectrum in the low energy region, one can clearly distinguish peaks above a continuous spectrum, which is consistent with the expected contribution of the electron capture branch of ^{204}Tl decay. In Figure 13, these peaks have been fitted and removed from the beta spec-

trum, which has then been unfolded.

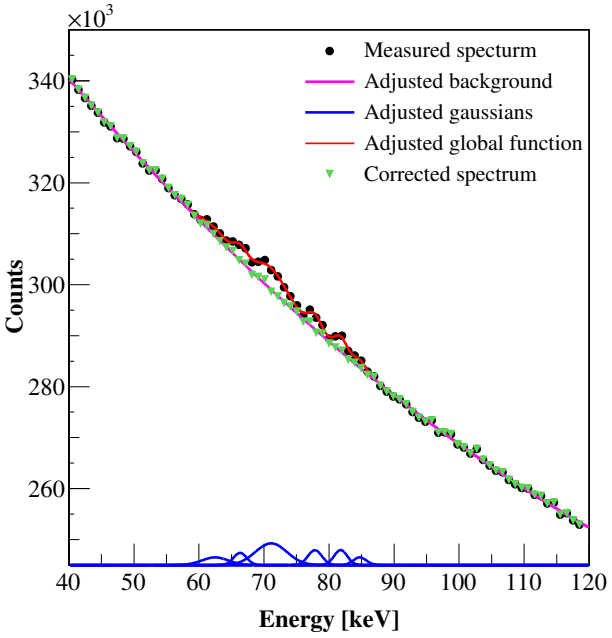

Figure 13: Removing peaks in ^{204}Tl β spectrum that are due to the contribution of the electron capture branch in the decay.

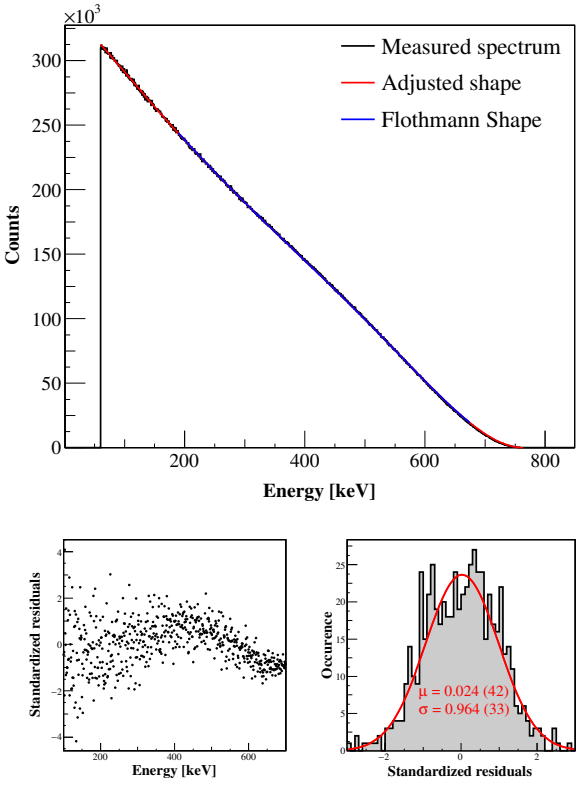

Figure 14: Adjusted ^{204}Tl spectrum (red) on the corrected, unfolded quasi-4π Silicon spectrum from this work (black). Adjusted spectrum determined in [48] is shown in their measured energy range (blue) for comparison. The shape from this work has been fitted between 100 and 700 keV starting from an allowed shape. Corresponding residuals are given at the bottom.

This corrected, unfolded spectrum is presented in Figure 14. It has been cut at 60 keV because its shape is questionable below due to the removal of the peaks above. It is compared to the spectrum built with the experimental shape factor determined in [48]. The two measurements are consistent in their common energy range, an agreement quantified below in the shape factor analysis.

The theoretical shape factor of this first forbidden unique transition depends on the momenta of both the β and ν particles:

$$C(W) = q^2 + \lambda_2 p^2 \tag{11}$$

where λ_2 is an energy-dependent parameter calculated from the Coulomb amplitudes of the relativistic electron wave functions [35]. As the ν momentum depends on E_0, the Kurie plot Eq. 9 has to be modified in order to introduce $C(W)$ in the fit:

$$\sqrt{\frac{N_{\rm exp}}{pWF(Z,W)}} = K\sqrt{(q^2 - B''q)\times(q^2+\lambda_2 p^2)} \tag{12}$$

with $B'' = 340$ eV for ^{204}Tl from the fit given in [47].

The energy resolution of the detection system has been taken into account as in the analysis of ^{14}C spectrum. A reasonable energy range of [650,760] keV has been considered when fitting the Kurie plot to determine the central value of the maximum energy. The dominant uncertainty component is from the fit because of the statistics of the measurement. The uncertainty due to the energy range has been estimated by varying the limits between 500 and 763 keV. The uncertainty due to the choice of the Fermi function was found to be negligible, and the central value has been determined with $F_0 L_0^*$. The maximum energy from our measurement is then $E_0 = 763.7\ (22)$ keV, fully consistent with the recommended AME2020 Q-value.

As in the analysis of the ^{14}C spectrum shape, the shape factor has been extracted fixing E_0 to the AME2020 Q-value. The method is identical and the shape factor from [48] has been considered:

$$C(W) = dq^2 + \lambda_2 p^2 \tag{13}$$

with d the parameter to be adjusted. In a first attempt, the spectrum has been fitted in the same energy range as in [48], i.e. in [190,675] keV, with an analytical Fermi function F_0 and without radiative corrections. Remarkably, the same value $d = 1.097$ has been obtained. A larger energy range has next been considered from 100 to 700 keV, what avoids the influence of possible non-linearities at the edge of the spectrum. The total uncertainty has been determined by adding in quadrature the fit uncertainty, the variation according to the Fermi functions and to the use of the radiative

corrections, and a component due to the energy range. The latter has been estimated by considering the energy range of [48] as a lower limit and a wide range from 60 to 750 keV as an upper limit. Considering F_0 and no radiative corrections, a value $d = 1.095\ (7)$ has been determined, fully consistent with the result of $d = 1.097\ (8)$ from [48]. A slightly better adjustment has been obtained, especially at low energy, considering $F_0 L_0$ and no radiative corrections, with a value of $d = 1.075\ (7)$. This adjusted spectrum is shown in Figure 14 with the corresponding residuals in the fit energy range. The agreement with the measured spectrum is excellent, with a disagreement parameter $(1 - R^2) = 0.0096\%$. The residuals are well centered around zero within 2σ but a slight non-linear trend can still be observed, which would needed further investigation.

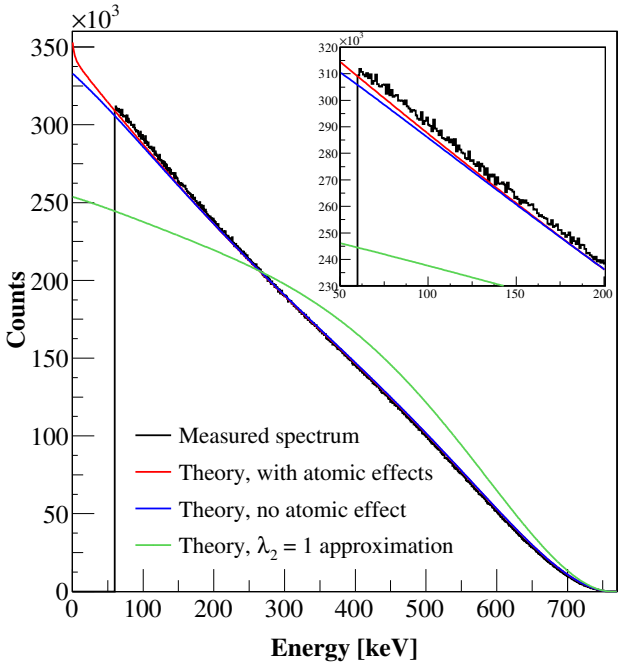

Figure 15: Corrected, unfolded ^{204}Tl β spectrum compared to different theoretical calculations.

Finally, we compare in Figure 15 our measurement to theoretical predictions calculated according to different assumptions. A usual approximation in the treatment of first forbidden unique transitions is to set $\lambda_2 = 1$ [10], which is clearly not able to reproduce the experimental ^{204}Tl spectrum. Calculating the spectrum as in Eq. 1 without atomic effects leads to a rather good description but part of the low-energy counts are missed. A more elaborated calculation has been performed including the atomic screening and exchange effects. The latter gives the most significant contribution and has been calculated as in [1]. If part of the discrepancy is filled in, atomic effects do not seem be sufficient. The ^{204}Tl β transition appears to be very sensitive to the λ_2 parameter and thus to the relativistic electron wave functions of the continuum states. If the experimental shape is confirmed at low energy, a more accurate theoretical description could be needed.

6. Conclusion

A detection system has been developed to precisely measure the shape of β spectra from at least 25 to 850 keV. As electrons highly diffuse in the matter, the geometry has been optimized up to a quasi-4π sr solid angle: the emitted particles from the radioactive source deposit their kinetic energy within two Silicon detectors in a very compact configuration. Ultra-thin radioactive sources have been prepared on purpose in order to minimize self-absorption. An unfolding method based on mono-energetic Monte Carlo simulations has been implemented to correct the measured spectra from the remaining distortions. The device has been characterised by the conversion electron peaks from ^{109}Cd and ^{207}Bi decays.

The ^{14}C and ^{204}Tl β spectra have been studied. The measured, unfolded spectra have been compared to precise measurements available in the literature and excellent agreement has been found in the common energy ranges. The maximum energies have been extracted and are fully consistent with the recommended AME2020 Q-values, though less precise. Analysing the ^{14}C spectrum, a linear slope has been determined to be $a = -0.430\ (23)\ \mathrm{MeV}^{-1}$, fully consistent with the best theoretical predictions of the weak magnetism term. Regarding ^{204}Tl, the knowledge of the spectrum has been extended from 63% in [48] to 92% in this work, down to 60 keV. A shape factor $(dq^2 + \lambda_2 p^2)$ has been extracted with $d = 1.075\ (7)$. A slight discrepancy with theoretical predictions has been highlighted at low energy.

A tenuous non-linear trend in the residuals, though statistically hardly meaningful, is still present and would deserve further investigation. One of the possibilities could be to improve the correction of the influence of the radioactive source, what would require a better knowledge of the crystal sizes and distribution. The influence of the energy resolution is also quite large on the analysis. This could be solved by replacing the PIPS detectors by two Si(Li) detectors in the same configuration. The other advantage would be to have thicker active volumes that would allow a total absorption of electrons up to 3 MeV of kinetic energy. Finally, adding a γ-ray detector in coincidence is foreseen in order to tidily select the transitions of interest in complex decay schemes.

Acknowledgments

The authors are very grateful to their former colleague Didier Lacour who helped them in the realization of the ultra-thin radioactive sources.

References

[1] S. J. Haselschwardt, J. Kostensalo, X. Mougeot, J. Suhonen, Improved calculations of β decay backgrounds to new physics in liquid xenon detectors, Phys. Rev. C 102 (2020) 065501. doi:10.1103/PhysRevC.102.065501.

[2] A. Glick-Magid, C. Forssén, D. Gazda, D. Gazit, P. Gysbers, P. Navrátil, Nuclear ab initio calculations of ^{6}He β-decay for beyond the standard model studies, Physics Letters B 832 (2022) 137259. doi:10.1016/j.physletb.2022.137259.

[3] A. A. Sonzogni, E. A. McCutchan, A. C. Hayes, Dissecting reactor antineutrino flux calculations, Phys. Rev. Lett. 119 (2017) 112501. doi:10.1103/PhysRevLett.119.112501.

[4] R. Broda, P. Cassette, K. Kossert, Radionuclide metrology using liquid scintillation counting, Metrologia 44 (4) (2007) S36–S52. doi:10.1088/0026-1394/44/4/s06.

[5] K. Kossert, X. Mougeot, The importance of the beta spectrum calculation for accurate activity determination of ^{63}Ni by means of liquid scintillation counting, Applied Radiation and Isotopes 101 (2015) 40 – 43. doi:10.1016/j.apradiso.2015.03.017.

[6] G. Rudstam, K. Aleklett, Average beta and gamma energies of fission products, Tech. rep., NFL-7 (The Studsvik Science Research Laboratory) (1979).

[7] A. I. Kassis, Radiotargeting agents for cancer therapy, Expert Opinion on Drug Delivery 2 (6) (2005) 981–991, pMID: 16296803. doi:10.1517/17425247.2.6.981.

[8] V. V. Kuzminov, N. J. Osetrova, Precise measurement of 14C beta spectrum by using a wall-less proportional counter, Physics of Atomic Nuclei 63 (7) (2000) 1292–1296. doi:10.1134/1.855786.

[9] M. Reich, H. Schüpferling, Formfaktor des Spektrums von ^{99}Tc, Z. Physik 271, 107 (1974). doi:10.1007/BF01676381.

[10] X. Mougeot, Reliability of usual assumptions in the calculation of β and ν spectra, Phys. Rev. C 91 (2015) 055504. doi:10.1103/PhysRevC.91.055504.

[11] N. Gove, M. Martin, Log-f tables for beta decay, Atomic Data and Nuclear Data Tables 10 (3) (1971) 205–219. doi:10.1016/S0092-640X(71)80026-8.

[12] M. R. Bhat, Evaluated nuclear structure data file (ensdf), in: S. M. Qaim (Ed.), Nuclear Data for Science and Technology, Springer, Berlin, Heidelberg, 1992, pp. 817–821. doi:10.1007/978-3-642-58113-7_227.

[13] M. A. Kellett, O. Bersillon, The decay data evaluation project (DDEP) and the JEFF-3.3 radioactive decay data library: Combining international collaborative efforts on evaluated decay data, EPJ Web of Conferences 146 (2017) 02009. doi:10.1051/epjconf/201714602009.

[14] X. Mougeot, Betashape: A new code for improved analytical calculations of beta spectra, EPJ Web Conf. 146 (2017) 12015. doi:10.1051/epjconf/201714612015.

[15] K. Kossert, M. Loidl, X. Mougeot, M. Paulsen, P. Ranitzsch, M. Rodrigues, High precision measurement of the ^{151}Sm beta decay by means of a metallic magnetic calorimeter, Applied Radiation and Isotopes 185 (2022) 110237. doi:10.1016/j.apradiso.2022.110237.

[16] A. Singh, Metrological study of the shape of beta spectra and experimental validation of theoretical models, Thesis, Université de Strasbourg (Sep 2020).
URL https://tel.archives-ouvertes.fr/tel-03176473

[17] Mirion Technologies. https://www.mirion.com/products/passivated-implanted-planar-silicon-pips-detectors (2022).

[18] SOLIDWORKS, Dassault Systèmes. https://www.solidworks.com/ (2022).

[19] A. Singh, X. Mougeot, B. Sabot, D. Lacour, A. Nourreddine, Beta spectrum measurements using a quasi-4π detection system based on si detectors, Applied Radiation and Isotopes 154 (2019) 108897. doi:10.1016/j.apradiso.2019.108897.

[20] A1422H Charge Sensitive Preamplifiers, CAEN. https://www.caen.it/products/a1422h/ (2022).

[21] LabZY nanoMCA module, Yantel. https://www.yantel.com/products/nanomca/ (2022).

[22] L. Feldman, C. S. Wu, Investigation of the beta-spectra of ^{10}Be, ^{40}K,^{99}Tc and ^{36}Cl, Phys. Rev. 87 (6) (1952) 1091–1099. doi:10.1103/physrev.87.1091.

[23] F. Juget, G. Lorusso, G. Haefeli, Y. Nedjadi, F. Bochud, C. Bailat, Development and validation of a double focalizing magnetic spectrometer for beta spectrum measurements, Nuclear Instruments and Methods in Physics Research Section A: Accelerators, Spectrometers, Detectors and Associated Equipment 942 (2019) 162384. doi:10.1016/j.nima.2019.162384.

[24] T. Branger, C. Bobin, M.-G. Iroulart, M.-C. Lépy, I. L. Garrères, S. Morelli, D. Lacour, J. Plagnard, Comparative study of two drying techniques used in radioactive source preparation: Freeze-drying and evaporation using hot dry nitrogen jets, Applied Radiation and Isotopes 66 (6-7) (2008) 685–690. doi:10.1016/j.apradiso.2008.02.063.

[25] F. Salvat, J. Fernandez-Varea, J. Sempau, PENELOPE-2014: A Code System for Monte Carlo Simulation of Electron and Photon Transport, OECD/NEA Data Bank, NEA/NSC/DOC(2015) 3, Issy-les-Moulineaux, France (2015).
URL https://www.oecd-nea.org/upload/docs/application/pdf/2020-01/nsc-doc2015-3.pdf

[26] M.-M. Bé, V. Chisté, C. Dulieu, M. Kellett, X. Mougeot, A. Arinc, V. Chechev, N. Kuzmenko, T. Kibédi, A. Luca, A. Nichols, Table of Radionuclides, Vol. 8 of Monographie BIPM-5, Bureau International des Poids et Mesures, Pavillon de Breteuil, F-92310 Sèvres, France, 2016.
URL http://www.bipm.org/utils/common/pdf/monographieRI/Monographie_BIPM-5_Tables_Vol8.pdf

[27] M.-M. Bé, V. Chisté, C. Dulieu, X. Mougeot, E. Browne, V. Chechev, N. Kuzmenko, F. Kondev, A. Luca, M. Galán, A. Nichols, A. Arinc, X. Huang, Table of Radionuclides, Vol. 5 of Monographie BIPM-5, Bureau International des Poids et Mesures, Pavillon de Breteuil, F-92310 Sèvres, France, 2010.
URL http://www.bipm.org/utils/common/pdf/monographieRI/Monographie_BIPM-5_Tables_Vol5.pdf

[28] H. Ruellan, M. Lépy, M. Etcheverry, J. Plagnard, J. Morel, A new spectra processing code applied to the analysis of ^{235}U and ^{238}U in the 60 to 200 keV energy range, Nuclear Instruments and Methods in Physics Research Section A: Accelerators, Spectrometers, Detectors and Associated Equipment 369 (2-3) (1996) 651–656. doi:10.1016/s0168-9002(96)80070-2.

[29] M. Wang, W. Huang, F. Kondev, G. Audi, S. Naimi, The AME 2020 atomic mass evaluation (II). Tables, graphs and references, Chinese Physics C 45 (3) (2021) 030003. doi:10.1088/1674-1137/41/3/030003.

[30] M.-M. Bé, V. Chisté, C. Dulieu, X. Mougeot, V. Chechev, F. Kondev, A. Nichols, X. Huang, B. Wang, Table of Radionuclides, Vol. 7 of Monographie BIPM-5, Bureau International des Poids et Mesures, Pavillon de Breteuil, F-92310 Sèvres, France, 2013.
URL http://www.bipm.org/utils/common/pdf/monographieRI/Monographie_BIPM-5_Tables_Vol7.pdf

[31] M.-M. Bé, V. Chisté, C. Dulieu, E. Browne, V. Chechev, N. Kuzmenko, R. Helmer, A. Nichols, E. Schönfeld, R. Dersch, Table of Radionuclides, Vol. 1 of Monographie BIPM-5, Bureau International des Poids et Mesures, Pavillon de Breteuil, F-92310 Sèvres, France, 2004.
URL http://www.bipm.org/utils/common/pdf/monographieRI/Monographie_BIPM-5_Tables_Vol2.pdf

[32] M. S. Rahman, G. Cho, Unfolding low-energy gamma-ray spectrum obtained with NaI(tl) in air using matrix inversion method, Journal of Scientific Research 2 (2) (2010) 221–226. doi:10.3329/jsr.v2i2.4372.

[33] M. Paulsen, K. Kossert, J. Beyer, An unfolding algorithm for high resolution microcalorimetric beta spectrometry, Nuclear Instruments and Methods in Physics Research Section A: Accelerators, Spectrometers, Detectors and Associated Equipment 953 (2020) 163128. doi:10.1016/j.nima.2019.163128.

[34] W. M. Visscher, R. A. Ferrell, Beta decay of ^{14}C and nuclear forces, Phys. Rev. 107 (3) (1957) 781–796. doi:10.1103/physrev.107.781.

[35] H. Behrens, W. Bühring, Electron radial wave functions and nuclear beta-decay, Oxford, Clarendon press, 1982.

[36] I. S. Towner, J. C. Hardy, New analysis of ^{14}O β decay: Branching ratios and conserved vector current consistency, Phys. Rev. C 72 (2005) 055501. doi:10.1103/PhysRevC.72.055501.

[37] R. M. F. Salvat, J. D. Martínez, J. Parellada, Analytical Dirac-Hartree-Fock-Slater screening function for atoms (Z = 1-92), Physical Review A 36 (1987) 467. doi:10.1103/PhysRevA.36.467.

[38] C. S. Cook, L. M. Langer, H. C. Price, Study of the beta-spectra of ^{14}C and ^{35}S, Phys. Rev. 74 (5) (1948) 548–552. doi:10.1103/physrev.74.548.

[39] S. D. Warshaw, The β-spectrum of ^{14}C, Phys. Rev. 80 (1) (1950) 111–112. doi:10.1103/physrev.80.111.

[40] A. Moljk, S. C. Curran, Beta spectra of ^{14}C and ^{35}S, Phys. Rev. 96 (2) (1954) 395–398. doi:10.1103/physrev.96.395.

[41] F. E. Wietfeldt, E. B. Norman, Y. D. Chan, M. T. F. da Cruz, A. García, E. E. Haller, W. L. Hansen, M. M. Hindi, R.-M. Larimer, K. T. Lesko, P. N. Luke, R. G. Stokstad, B. Sur, I. Žlimen, Further studies on the evidence for a 17-kev neutrino in a ^{14}doped germanium detector, Phys. Rev. C 52 (1995) 1028–1040. doi:10.1103/PhysRevC.52.1028.

[42] G. Alimonti, G. Angloher, C. Arpesella, M. Balata, G. Bellini, J. Benziger, S. Bonetti, L. Cadonati, F. Calaprice, G. Cecchet, M. Chen, N. Darnton, A. de Bari, M. Deutsch, F. Elisei, F. von Feilitzsch, C. Galbiati, F. Gatti, M. Giammarchi, D. Giugni, T. Goldbrunner, A. Golubchikov, A. Goretti, T. Hagner, F. Hartmann, R. von Hentig, G. Heusser, A. Ianni, J. Jochum, M. Johnson, M. Laubenstein, P. Lombardi, S. Magni, S. Malvezzi, I. Manno, G. Manuzio, F. Masetti, U. Mazzucato, E. Meroni, M. Neff, A. Nostro, L. Oberauer, A. Perotti, A. Preda, R. Raghavan, G. Ranucci, E. Resconi, M. Ruscitti, R. Scardaoni, S. Schönert, O. Smirnov, R. Tartaglia, G. Testera, P. Ullucci, R. Vogelaar, S. Vitale, O. Zaimidoroga, Measurement of the ^{14}C abundance in a low-background liquid scintillator, Phys. Lett. B 422 (1-4) (1998) 349–358. doi:10.1016/s0370-2693(97)01565-7.

[43] L. G. Smith, A. H. Wapstra, Masses of isotopes of H, He, C, N, O, and F, Phys. Rev. C 11 (1975) 1392–1400. doi:10.1103/PhysRevC.11.1392.

[44] F. P. Calaprice, B. R. Holstein, Weak magnetism and the beta spectra of ^{12}B and ^{12}N, Nuclear Physics A 273 (2) (1976) 301–325. doi:10.1016/0375-9474(76)90593-5.

[45] A. García, B. A. Brown, Shape of the β spectra in the A=14 system, Phys. Rev. C 52 (6) (1995) 3416–3427. doi:10.1103/physrevc.52.3416.

[46] M. Loidl, J. Beyer, L. Bockhorn, C. Enss, S. Kempf, K. Kossert, R. Mariam, O. Nähle, M. Paulsen, P. Ranitzsch, M. Rodrigues, M. Schmidt, Beta spectrometry with metallic magnetic calorimeters in the framework of the european empir project metrobeta, Applied Radiation and Isotopes 153 (2019) 108830. doi:10.1016/j.apradiso.2019.108830.

[47] L. Hayen, N. Severijns, K. Bodek, D. Rozpedzik, X. Mougeot, High precision analytical description of the allowed β spectrum shape, Rev. Mod. Phys. 90 (2018) 015008. doi:10.1103/RevModPhys.90.015008.

[48] D. Flothmann, W. Wiesner, R. Löhken, H. Rebel, β-spektroskopie mit Halbleiterdetektoren beim Zerfall von ^{32}P,^{49}Sc, ^{204}Tl und ^{210}Bi, Zeitschrift für Physik A Hadrons and nuclei 225 (2) (1969) 164–194. doi:10.1007/bf01392517.